Interstitial flow influences direction of tumor cell migration through competing mechanisms

William J. Polacheck[a], Joseph L. Charest[b], and Roger D. Kamm[a,c,1]

Departments of [a]Mechanical Engineering and [c]Biological Engineering, Massachusetts Institute of Technology, Cambridge, MA 02139; and [b]The Charles Stark Draper Laboratory, Cambridge, MA 02139

Edited* by Shu Chien, University of California at San Diego, La Jolla, CA, and approved May 24, 2011 (received for review March 9, 2011)

Interstitial flow is the convective transport of fluid through tissue extracellular matrix. This creeping fluid flow has been shown to affect the morphology and migration of cells such as fibroblasts, cancer cells, endothelial cells, and mesenchymal stem cells. A microfluidic cell culture system was designed to apply stable pressure gradients and fluid flow and allow direct visualization of transient responses of cells seeded in a 3D collagen type I scaffold. We used this system to examine the effects of interstitial flow on cancer cell morphology and migration and to extend previous studies showing that interstitial flow increases the metastatic potential of MDA-MB-435S melanoma cells [Shields J, et al. (2007) *Cancer Cell* 11:526–538]. Using a breast carcinoma line (MDA-MB-231) we also observed cell migration along streamlines in the presence of flow; however, we further demonstrated that the strength of the flow as well as the cell density determined directional bias of migration along the streamline. In particular, we found that cells either at high seeding density or with the CCR-7 receptor inhibited migration against, rather than with the flow. We provide further evidence that CCR7-dependent autologous chemotaxis is the mechanism that leads to migration with the flow, but also demonstrate a competing CCR7-independent mechanism that causes migration against the flow. Data from experiments investigating the effects of cell concentration, interstitial flow rate, receptor activity, and focal adhesion kinase phosphorylation support our hypothesis that the competing stimulus is integrin mediated. This mechanism may play an important role in development of metastatic disease.

mechanobiology | computational model | signaling | cell mechanics

Tissues are composed of cells residing in an extracellular matrix (ECM) containing interstitial fluid that transports nutrients and signaling molecules (1, 2). Osmotic and hydrostatic pressure gradients across tissues resulting from physiologic processes such as drainage toward lymphatics, inflammation, locally elevated pressures due to tumor growth or leaky microvessels, and muscle contraction each drive fluid flow through the ECM (2, 3). This fluid flow is termed interstitial flow and has long been recognized to be instrumental in tissue transport and physiology (1, 4, 5). Chary and Jain used fluorescence recovery after photobleaching to directly observe fluid flow in the tissue interstitium and determined typical flow velocities to be on the order of 0.1–2.0 μm/s, and more recent studies have demonstrated that flow can reach velocities as high as 4.0 μm/s (6, 7).

Interstitial flow is particularly important in driving transport in the vicinity of tumors, as neoplastic tissue is often characterized by localized increases in interstitial pressure, leading to high interstitial pressure gradients at the tumor margin (8). Interstitial flow has hence emerged as a possible stimulus for guiding tumor cell migration in the formation of metastases (9–12).

Shields et al. observed increased metastatic potential in cell populations exposed to flow and demonstrated that this increase in metastatic potential was activated through binding of self-secreted CCL21 ligand to the CCR7 receptor (13). This autocrine signaling mechanism, termed autologous chemotaxis, arises in a flow field where convection distributes autocrine chemokine factors creating a transcellular chemokine gradient, which in turn provides a chemotactic signal. For CCL21 at physiologically relevant flow velocities, flow increases the concentration of ligand at the downstream side of the cell, providing a positive downstream chemotactic signal (14).

The transwell assay used by Shields et al. to develop the autologous chemotaxis model and other similar in vitro assays have provided valuable insight into the metastatic process and tumor cell migration by allowing the systematic study of isolated stimuli on tumor cells (9, 10, 15–19). However, recent work has demonstrated that focal adhesion (FA) formation and regulation are a function of dimensionality of cell culture (20), and previous work has demonstrated FA formation is important in regulating endothelial cell (EC) response to laminar shear stress (21). Further verification of the autologous chemotaxis model and investigation of other flow-induced cell stimuli would clearly benefit from a cell culture system in which cells are seeded in a physiologically relevant 3D matrix and in which the time-dependent morphological and migratory responses to flow can be quantified. 3D culture systems have been used to demonstrate the effect of interstitial flow on other cell types, such as fibroblasts (19, 3), myofibroblasts (22), endothelial cells (16), and smooth muscle cells (18).

We developed a microfluidic cell culture system in which the directional bias and dynamics of cell migration in a physiologically relevant 3D matrix can be observed and quantified, and we used this system to investigate the effects of interstitial flow on tumor cell migration. We demonstrate that interstitial flow influences the directional bias of cell migration and that the migratory response is flow rate and cell density dependent. Furthermore, by blocking the CCR7 pathway, we provide evidence to support the CCR7-dependent autologous chemotaxis model for migration in the direction of flow, and we demonstrate that a second, CCR7-independent pathway stimulates cells to migrate against the flow. We found that this upstream stimulus is cell density independent and that flow induces phosphorylation of focal adhesion kinase (FAK) at Tyr-397, and we hypothesize that flow-induced tension in integrins provides the upstream migratory stimulus. Competition between these two apparently independent mechanisms largely determines the direction of cell migration under the influence of interstitial flow.

Results

Cell Culture System Design and Verification of Interstitial Flow Field. We used a microfluidic cell culture system to culture breast cancer cells (MDA-MB-231) in a 3D collagen I matrix and to subject these cells to a controlled level of interstitial flow. MDA-MB-231 cells are known to express CCR7 (23, 24) and migrate

Author contributions: W.J.P., J.L.C., and R.D.K. designed research; W.J.P. performed research; W.J.P. and R.D.K. analyzed data; and W.J.P. and R.D.K. wrote the paper.

The authors declare no conflict of interest.

*This Direct Submission article had a prearranged editor.

[1]To whom correspondence should be addressed. E-mail: rdkamm@mit.edu.

This article contains supporting information online at www.pnas.org/lookup/suppl/doi:10.1073/pnas.1103581108/-/DCSupplemental.

toward increasing concentration of CCL21 when cultured in 2D and exposed to a CCL21 gradient (25). The system consists of two channels separated by a region containing single cells suspended in a collagen I gel (Fig. 1*A*). By applying a hydrostatic pressure gradient across the gel region, a consistent flow field is generated. Finite element model (FEM) software was used to solve Brinkman's equation for flow through porous medium for our system geometry (26) (Fig. 1*B* and *SI Materials and Methods*). We validated the flow field by adding fluorescent microspheres to the bulk fluid and imaging the microspheres using fluorescent time-lapse microscopy (Fig. 1*B*). Interstitial flow velocities were found to be repeatable and consistent with numerical predictions (Fig. 1*C*); the measured and predicted velocity vectors were also observed to be codirectional (Fig. 1*D*). In what follows, each flow field is referred to by its respective nominal value, the rounded means of 0.3 μm/s and 3.0 μm/s, respectively, which are representative of the range of published in vivo interstitial flow velocity values (7, 8). From the bead tracking data, the hydraulic permeability of 2 mg/mL collagen I gel was determined to be 1×10^{-13} m^2, similar to previously published values (18, 19).

Cells Seeded at High Concentration Migrate Against the Flow. The cells were suspended in 3D within the gel and migrated in 3D (Fig. 2*A* and *SI Materials and Methods*). Confocal reflectance microscopy demonstrated that the cells degraded the collagen matrix as they migrated, leaving tracks in the gel during migration, thus suggesting a proteolytically active migration mechanism (Fig. S1*A*). When exposed to interstitial flow, breast cancer cells cultured in 3D aligned parallel to flow streamlines (Fig. S1);

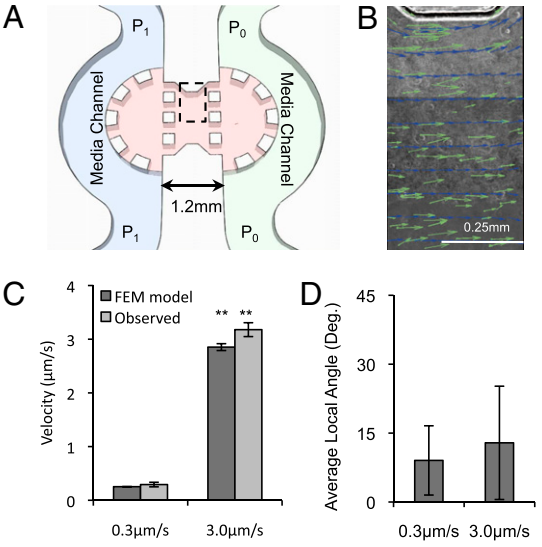

Fig. 1. Microfluidic cell culture system for investigating the effects of interstitial flow on tumor cell migration. (*A*) Schematic of the microfluidic device. The device consists of two channels (P_1 and P_0) separated by a region in which cells are suspended in collagen I gel. By applying a pressure gradient across the gel, a consistent flow field is generated. To validate the flow field, fluorescent microspheres were introduced into the bulk media, and time-lapse images were taken to track the beads. (*B*) Velocity vectors observed by tracking the fluorescent microspheres (green) superimposed on streamline vectors for a computation model (blue) and on a composite phase contrast image of the region of the device indicated by the dashed line in *A*. The composite phase contrast image is comprised of subregions that were imaged sequentially to measure velocity throughout the whole gel region. (*C* and *D*) Experimentally observed velocity vectors are similar to the velocity vectors predicted by the FEM in (*C*) magnitude and (*D*) direction, measured by the average of the local angles between observed streamline vectors and the predicted streamline vectors (mean ± SEM, $^{**}P < 0.01$ between flow velocities; average angle computed between 0° and 90°).

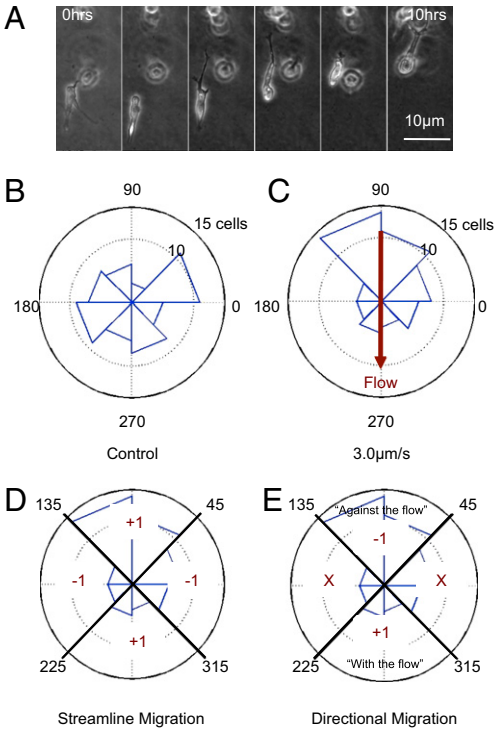

Fig. 2. Interstitial flow influences direction of cell migration. (*A*) Sample time-lapse images of a cell migrating in an interstitial flow field. Flow is 3.0 μm/s from top to bottom in the image. (*B*) Sample data from one control device. The polar histogram demonstrates distribution of angles of net migration vectors for cells in a population in one device. Cells in control devices without flow migrate randomly. (*C*) Flow changes the distribution of migration vector angles. In this sample data from one device, cell migration bias, are against the flow. To quantify directional bias in cell migration, two metrics were computed: (*D*) The streamline migration metric is a measure of migration bias along the streamlines, and (*E*) the directional migration metric is a measure of the upstream or downstream migration bias for cells migrating along streamlines. "X" indicates that cells not migrating along streamlines are not scored for the directional migration metric.

this cell alignment to flow in 3D is similar to the alignment of endothelial cells cultured in 2D, reported by Levesque and Nerem (27), although the mechanisms of alignment might well differ. Using time-lapse imaging over 16-h intervals, the center of mass of each cell was tracked 24 h after seeding and within 30 min of applying interstitial flow. Cell migration speed was found to be independent of interstitial flow magnitude (0.10 μm/min ± 0.05, Fig. S2*A*). Cells exposed to interstitial flow migrated with increased directionality, defined as the magnitude of the vector from original to final cell location at 24 h normalized by the sum of the magnitude of migration vectors determined every 15 min (0.63 ± 0.073 for 0.3 μm/s and 0.61 ± 0.071 for 3.0 μm/s, compared with 0.39 ± 0.071 for control, Fig. S2*B*); however, cell motility, defined as the percentage of cells migrating a distance greater than one cell diameter in 8 h, was unaffected by flow (Fig. S3*C*).

Interstitial flow induced a directional bias in cellular migration. Polar histograms of migration data for a control device and a device with 3.0 μm/s flow clearly demonstrate the effect of flow on the direction of migration vectors (Fig. 2). In devices with flow, cells preferentially migrated along streamlines. To quantify the migration direction of cell populations, two metrics are presented. The "streamline migration metric" scores cells with a +1 if they migrate within 45° of a streamline and a −1 if they migrate outside of this zone (Fig. 2*D*). An average score for a cell population of +1 indicates that all of the cells are migrating along

a streamline, a score of 0 corresponds to purely random migration, and score of −1 indicates that all cells are migrating perpendicular to the streamline. To determine directional bias of migration along streamlines, a "directional migration metric" was computed that scored cells with a +1 if they migrated within 45° of a streamline in the downstream direction (subsequently denoted "with the flow") and a −1 if they migrated within 45° of a streamline in the upstream direction (subsequently denoted "against the flow") (Fig. 2*E*). A population has an average score of +1 if all of the cells migrating within 45° of a streamline are migrating with the flow, a score of −1 if all of the cells are migrating against the flow, and a score of 0 if equal numbers of cells are migrating with and against the flow.

Cells seeded at 25×10^4 cells/mL and exposed to interstitial flow preferentially migrated along the flow streamlines, with average streamline migration scores of 0.47 ± 0.06 for 0.3 μm/s and 0.24 ± 0.04 for 3.0 μm/s (mean ± SD, Fig. 3*A*). Of the cells migrating along the streamline, a greater fraction of the cell population migrated upstream than downstream and the strength of this upstream bias was a function of interstitial flow rate. At an interstitial flow speed of 0.3 μm/s, the average directional migration score was −0.27 ± 0.17, and at 3.0 μm/s directional bias increased further to −0.40 ± 0.08. Cells in control devices did not preferentially migrate in either direction (Fig. 3*B*). These MDA-MB-231 cells migrate in the opposite direction of the MDA-MB-435S cells exposed to 0.2 μm/s flow in a transwell system as reported by Shields et al. (13).

At Low Cell Seeding Density, Cells Migrate with the Flow. To test for the effect of cell density on directional migration under flow, experiments were conducted at two different seeding densities, 25×10^4 and 5×10^4 cells/mL. Decreasing cell concentration did not affect the bias for migration along streamlines in a 0.3-μm/s interstitial flow field, although a smaller percentage of cells migrated along streamlines in a 3.0-μm/s interstitial field when seeded at a lower concentration (Fig. 3*A*).

Decreasing cell density did, however, exert a dramatic effect on the direction of migration, causing a reversal in the directional bias of migration relative to the flow as indicated by the sign change in the directional migration metric, a result consistent with Shields et al. (13). At a flow speed of 0.3 μm/s, the average directional migration score was −0.27 ± 0.17 at 25×10^4 cells/mL but increased to 0.570 ± 0.18 at 5×10^4 cells/mL. For 3.0 μm/s, the average directional migration score was −0.401 ± 0.08 at 25×10^4 cells/mL but increased to 0.307 ± 0.16 at 5×10^4 cells/mL (Fig. 3*B*).

Blocking CCR7 Signaling Increases the Tendency for Upstream Migration. In devices seeded at 25×10^4 cells/mL and subject to 0.3 μm/s interstitial flow, addition of CCR7 reduced the bias of migration along streamlines, lowering the average streamline migration metric from 0.472 ± 0.060 to 0.174 ± 0.070, but had little effect on cells in a 3.0-μm/s flow field (Fig. 3*A*). At both interstitial flow velocities, blocking CCR7 increased directional migration *against* the flow (Fig. 3*B*).

Cells at Low Seeding Density Migrate Upstream When CCR7 Signaling Is Blocked. Interestingly, the combined effect of decreasing cell density and blocking CCR7 resulted in a flow rate-dependent change in migration bias along streamlines. At 0.3 μm/s, the streamline migration score was reduced from 0.489 ± 0.122 to 0.201 ± 0.031 with the addition of CCR7 blocking antibody at 5×10^4 cells/mL; however, at 3.0 μm/s, the streamline migration score increased from 0.088 ± 0.188 to 0.384 ± 0.06 at 5×10^4 cells/mL (Fig. 3*A*).

In devices seeded at 5×10^4 cells/mL, addition of anti-CCR7 blocking antibody completely negated preferential migration in the direction of flow and, in fact, caused preferential migration against the flow. The average directional migration score dramatically decreased at both flow velocities, from 0.570 ± 0.12 to −0.420 ± 0.19 at 0.3 μm/s and from 0.307 ± 0.16 to −0.649 ± 0.18 at 3.0 μm/s (Fig. 3*B*).

Blocking CCR7 Eliminates Seeding Density Dependence of Cell Migration. When comparing cell populations at 5×10^4 cells/mL with CCR7 blocking antibody and populations at 25×10^4 cells/mL with CCR7 blocking antibody, there are no significant differences in directional migration bias. These data suggest that addition of the blocking antibody negates the effect of cell concentration on directional migration bias. Furthermore,

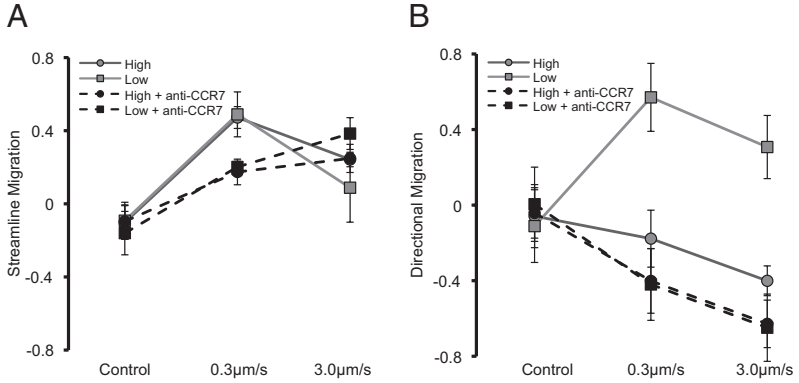

Fig. 3. Interstitial flow induces a bias in direction of tumor cell migration. "High" and "low" refer to seeding densities of 25×10^4 cells/mL and 5×10^4 cells/mL, respectively. (*A*) Streamline migration (see Fig. 2*D* for definition) measures the bias in migration along streamlines of a cell population. Cells exposed to interstitial flow preferentially migrated along streamlines, and this bias is a function of flow rate, cell density, and CCR7 receptor activity. Blocking CCR7 in a 0.3-μm/s flow field causes a significant decrease in streamline migration score ($P < 0.01$). In a 3.0-μm/s flow field, blocking CCR7 has the opposite effect of increasing streamline migration score, but only at a low cell density ($P < 0.05$). (*B*) Directional migration (see Fig. 2*E* for definition) demonstrates directional bias of cells migrating along the streamline, positive directional migration indicates downstream migration, and positive streamline migration indicates cells are preferentially migrating along the streamline. Cells exposed to interstitial flow preferentially migrated upstream or downstream as a function of flow rate, cell density, and CCR7 receptor activity. Directional migration scores become more negative with increasing flow velocity. With active CCR7, increasing cell density reverses directional bias from downstream to upstream ($P < 0.01$ for both flow rates), but when CCR7 is blocked, directional migration scores are more negative and do not depend on cell density. (Mean ± SD was computed by averaging the score for each cell in one device ($n > 15$) and averaging the score for three devices at each condition.)

although the effects are not statistically significant ($P = 0.17$ for 5×10^4 cells/mL and $P = 0.3$ for 25×10^4 cells/mL), a consistent trend is observed in the effect of flow rate. At both cell concentrations, increasing the flow rate from 0.3 μm/s to 3.0 μm/s tended to increase the upstream migration bias of cells migrating along the streamline (for 5×10^4 cells/mL, directional migration decreased from 0.570 ± 0.12 to 0.307 ± 0.16, and for 25×10^4 cells/mL, directional migration decreased from -0.27 ± 0.17 to -0.401 ± 0.08; Fig. 3).

Interstitial Flow Increases FAK Activation. In devices seeded at 25×10^4 cells/mL, cells exposed to 3.0 μm/s flow demonstrated increased phosphorylation at Tyr-397 in FAK, which is associated with focal adhesion formation and Src kinase activation (28–30). The relative activation of FAK was determined by measuring the intensity of immunofluorescent staining for FAK and *p*-FAK(Y397) in control devices and in devices exposed to 3.0 μm/s flow, and cells exposed to flow demonstrated a significant increase in *p*-FAK(Y397) intensity (Fig. 4). High magnification confocal images demonstrate that *p*-FAK(Y397) is localized to the cell membrane (Fig. S4). That flow results in increased FAK phosphorylation is consistent with data from experiments in which we blocked Src kinase by introducing a specific inhibitor of Src kinase PP2 (31, 32). We found that blocking Src kinase activity resulted in decreased upstream migration, and cells migrated randomly, with no biased migration upstream or downstream (Fig. S5).

Discussion

Effect of Interstitial Flow on Cell Migration. Interstitial flow influenced tumor cell migration and, in particular, dramatically affected the direction of migration. For all culture conditions with interstitial flow, cells preferentially migrated along streamlines. The relative fraction of the cell population that migrated along the streamlines, and the upstream and downstream bias along the streamline, was a function of cell density, CCR7 activity, and interstitial flow velocity.

CCR7 and Autologous Chemotaxis. For cells seeded at 5×10^4 and 25×10^4 cells/mL in 3.0-μm/s and 0.3-μm/s flow fields, addition of CCR7 blocking antibody decreased the tendency for downstream migration. These data indicate that the CCR7 receptor is involved in downstream migration and thus support the findings of Shields et al., who identified the CCR7 chemokine receptor as critical in the signaling pathway responsible for autologous chemotaxis (13). Autologous chemotaxis is the result of a flow-induced gradient of an autocrine chemotactic signal that is detected by the CCR7 chemokine receptor and stimulates migration in the direction of flow. Our data confirm that CCR7 is involved in tumor cell migration, and we provide validation for the autologous chemotaxis model by demonstrating that CCR7 is directly involved in downstream migration.

Interestingly, in experiments without the CCR7 blocking antibody, migration direction was a strong function of cell seeding density. As cell concentration was increased, fewer cells migrated downstream, and a general tendency for migration in the *upstream* direction began to emerge. We expect the density dependence in the direction of cell migration is the result of the interaction between autocrine and paracrine chemokine concentration fields. Autologous chemotaxis, as the result of autocrine chemokine gradients, had previously been studied in the context of single cells (14), but when we included the effects of neighboring cells in our model, we observed that increasing cell density decreases the magnitude of the transcellular gradient for cells downstream of other cells (Fig. 4 and *SI Materials and Methods*). The decrease in transcellular gradient magnitude is due to the fact that the local effects of a single cell become overwhelmed by the effects of ligand release from a population of cells. Consequently, increasing the cell density decreases the autocrine transcellular gradient, attenuating the signal for autologous chemotaxis and reducing the tendency for CCR7-mediated migration downstream. As further validation that high cell concentration results in a weaker autologous chemotaxis stimulus, the directional migration trends are similar between cell populations seeded at high cell concentration and cell populations with blocked CCR7.

Competing Signals. When CCR7 is blocked, directional migration scores decrease for all conditions tested. The decrease in streamline migration scores is pronounced for cells at 5×10^4 cells/mL; the average directional migration score changes sign from positive to negative, reflecting a shift in migration bias from downstream to upstream. Motivated by the negative directional migration scores for both cell densities and flow rates when CCR7 is blocked, we hypothesize that a CCR7-*independent* stimulus competes with CCR7-dependent autologous chemotaxis and when CCR7 is inhibited, stimulates cells to migrate upstream. The relative strength of these two stimuli governs the directional bias in migration for a cell population and is a function of cell density, interstitial flow rate, and CCR7 receptor availability.

The streamline and directional migration scores provide insight into the nature of the CCR7-independent stimulus. Directional migration scores monotonically decrease (become more negative) with increasing interstitial flow velocity, and this effect is independent of CCR7 activity and seeding density. In contrast, downstream migration of cells at low-density peaks at a flow rate of 0.3 μm/s then decreases at 3.0 μm/s. These data suggest that the CCR7-independent stimulus increases in strength with increasing interstitial flow velocity. Furthermore, when CCR7 is blocked, the directional migration score is independent of cell seeding density,

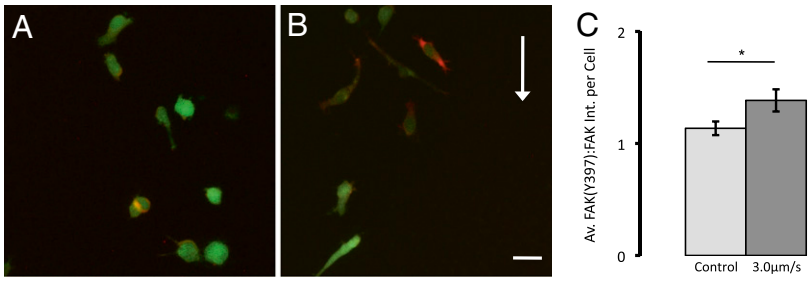

Fig. 4. Interstitial flow induces FAK phosphorylation. (*A* and *B*) Overlay of GFP in green and *p*-FAK(Y397) in red for projected confocal z-stacks of (*A*) a representative control device and (*B*) a representative device with 3.0 μm/s flow. Flow direction is from the top to the bottom of the image. Although each cell population demonstrated heterogeneity in FAK phosphorylation, on average, cells exposed to interstitial flow demonstrated increased FAK activation. (*C*) Normalized intensity ratio of *p*-FAK(Y397) to FAK per cell demonstrates increased FAK phosphorylation in cells exposed to flow. (Scale bar, 30 μm.) Mean ± SEM was computed by averaging total intensity of *p*-FAK(Y397) to FAK staining for $n > 50$ cells in three devices for each condition. *$P < 0.05$.

suggesting that the strength of the CCR7-independent stimulus is cell density independent. Interestingly, the upstream migration stimulus persists even at low cell density and flow rate, suggesting that the stimulus is independent of cell–cell interactions.

Pressure Gradient and Fluid Shear Stress. The stimulus that drives cells upstream is flow rate *dependent* but cell density *independent*. Flow-induced stresses on a cell are a function of flow rate and, in contrast to an autocrine or paracrine signaling stimulus, independent of cell density. Shear stress has long been known to play a role in EC migration (3, 33–36); however, in our system, cells are suspended in a 3D matrix, and the presence of this porous medium causes the force due to fluid pressure gradient across the cell to dominate the fluid shear force (37). By modeling a cell as a sphere embedded in a porous medium, we found the force due to the pressure drop across the cell (F_{pm}) relative to the shear stress imparted by the fluid (F_s) scales as

$$\frac{F_{pm}}{F_s} \sim \frac{R}{\sqrt{\kappa}}, \quad [1]$$

where R is the radius of the cell and κ is the permeability of the medium (*SI Materials and Methods*). Assuming the cell is a sphere of radius 10 μm and $\kappa = 1 \times 10^{-13}$ m^2, determined from the bead tracking data (*Results*), the stress due to pressure gradient across the cell can be determined from Brinkman's equation to be 1.3 Pa determined by an FEM for 3.0 μm/s flow rate (*SI Materials and Methods*).

Importantly, the force due to the flow-induced pressure drop across the cell is ~30 times as large as the integrated shear stress and ~0.4 nN—comparable to the total integrated shear stress on an endothelial cell in vivo (35). A total of 1.2 Pa shear stress has been shown to increase the affinity and avidity of αvβ3 integrins in endothelial cells (38, 39) and increase activation of FAK (33). For both endothelial cells in 2D and cancer cells in 3D, the force on the cell imparted by the fluid must be largely balanced by tension in the integrins that connect the cell to the surrounding matrix. Consequently, we expect that fluid-induced forces of this magnitude can activate integrins for cancer cells in 3D, driving focal adhesion activation (40–42). Furthermore, we expect the magnitude of force due to the pressure gradient to be greater on cells in vivo where the permeability is much lower than in collagen gel (1).

FAK Activation. Pressure forces from flow past a cell in a 3D matrix lead to a transcellular stress gradient (37), and this stress results in asymmetric force in cell–matrix interactions—e.g., tensile force on the upstream side and compressive force on the downstream side. Previous work demonstrates that FAK colocalizes with activated integrins and activates Src kinase (28, 29), which modulates traction forces important for tumor cell migration (43, 44).

Cells at a density and flow rate that induce upstream migration demonstrate increased FAK activation (Fig. 4). Because the upstream migration stimulus is independent of cell density and a function of flow rate, and the force due to fluid flow is large enough to induce integrin activation, we hypothesize that the increased FAK activation is due to flow-induced stress gradients and resulting integrin activation. These stress gradients presumably lead to a difference in integrin and FA activation, with more activation upstream, where cell–matrix connections are in tension. We expect that this mechanism driving upstream migration is similar to that examined by Lo et al., who demonstrated that a transcellular strain gradient, which presumably results in biased integrin activation due to the gradient in tension on the integrin receptors, guides cell migration toward increasing strain (45). Consistent with the hypothesis that flow-induced FAK activation drives upstream migration, we found that blocking Src kinase with PP2 reduced upstream migration (Fig. S4).

We expect that the difference in integrin distribution for cells on a 2D substrate and in a 3D matrix is primarily responsible for the differences between our data and previous reports, which have demonstrated polarized activation of FAK downstream during lamellipodia formation and subsequent downstream migration in endothelial monolayers (21). Lin and Helmke demonstrated that migration direction is a function of geometry and confluency and that nonconfluent endothelial cells undergo triphasic mechanotaxis, as opposed to endothelial cells in a confluent monolayer, which migrate downstream immediately upon application of shear flow (46). In addition to forces on the cell being pressure dominated rather than shear dominated for cells in 3D, recent work has demonstrated that migration in 3D is much different from 2D migration, and Fraley et al. have demonstrated that migration in 3D is predominantly governed by pseudopod activity and matrix deformation (20). Consistent with these data, confocal reflectance data support that cells in our devices are migrating in 3D, extending pseudopodia and leaving gaps in the matrix at the trailing edge as they migrate (Fig. S1*A*).

Interstitial flow has been studied extensively with regard to drug transport for cancer treatment (8), and in vivo it has been shown that interstitial fluid pressure (IFP) is correlated with survival of patients with cervical cancer (47) and reducing interstitial fluid pressure reduces tumor cell proliferation (11). Because interstitial fluid flows from a tumor to surrounding lymphatics or the low-pressure veins, blocking CCR7 and thus inhibiting migration in the flow direction would reduce migration from the tumor and likely reduce the probability of metastasis formation. Cell density and interstitial flow rates decrease with increasing distance from the tumor, both of which are highest at the tumor margin. Because high cell density and high flow rates both favor upstream migration, our data suggest the existence of an "escape radius" at a critical distance from the tumor surface. For cells at a radial distance less than the escape radius, interstitial flow guides cells upstream, keeping cells clustered with the tumor, but for cells located beyond the escape radius, interstitial flow guides cells downstream, toward draining lymphatics or veins. Although further modeling and in vivo data are required to validate this hypothesis, the escape radius could be a critical parameter in estimating the severity of metastatic disease and determining proper treatment. Interstitial flow is just one of many biochemical and biophysical stimuli in vivo that influences tumor cell migration, but its consideration is crucial for understanding and treating metastatic disease and for developing tissue-engineered constructs.

Materials and Methods

Cell Seeding. Microfluidic devices were fabricated using soft lithography in a process that has been described previously (16). MDA-MB-231 cells originally derived from a pleural effusion were obtained from the American Type Culture Collection and were cultured in standard growth media of 10× DMEM (Invitrogen) with 10% FBS (Invitrogen). Collagen type I (BD Biosciences) solution was buffered with 10× DMEM, titrated to a pH of 8.9 with NaOH, and brought to a final concentration of 2 mg/mL collagen I in total solution. Cells were harvested with 0.05% Trypsin/EDTA and centrifuged at 200 × *g* for 5 min. The cells were resuspended in media at the desired concentration, and the suspended cells were then mixed with collagen I solution to make a final cell density of 2.5×10^5 or 0.5×10^5 cells/(mL total solution).

Cells were incubated overnight at 37 °C. To apply a pressure gradient, external media reservoirs were connected to the microfluidic chip. Medium was added to each reservoir at volumes that established the desired pressure gradient across the gel (40-Pa pressure head for 3 μm/s flow). Devices were allowed to reach thermal equilibrium at 37 °C before imaging (see *SI Materials and Methods* for details on imaging and data quantification). Media were supplemented with human recombinant EGF at 10 ng/mL (PeproTech). For CCR7 blocking, anti-human CCR7 MAb (R&D Systems) was added to the media at 5 μg/mL.

Cell Tracking. Phase contrast images were taken every 15 min for 16–24 h in an environmental chamber held at 37 °C and 5% CO_2. Images were taken at a location >50 μm from the glass and polydimethylsiloxane (PDMS) surfaces to ensure imaged cells were suspended in 3D matrix and to ensure edge effects could be neglected, and imaging began within 30 min of applying the pressure gradient. After imaging, 200-nm diameter fluorescent microspheres (Polysciences) were added to the media, and fluorescent images were taken to ensure that the applied pressure head and flow had not induced gel rupture.

Fixation and Imaging. Cells were exposed to flow as described above for 1 h, before media were replaced with 4% paraformaldehyde to fix the cells. During fixation, the pressure head and flow were maintained in experimental devices to preserve protein expression and activation. Cells were then permeabilized and incubated with mouse anti-human FAK mAb (Abcam) and rabbit anti-human pAb FAK(Y397) (Abcam). Cells were subsequently imaged with a confocal laser-scanning microscope, and laser power and signal gains were maintain at constant level among all devices. The total intensity of FAK(Y397) was normalized to intensity of FAK for pixels colocalized to GFP for each cell. Interdevice variability for each condition was not significant.

ACKNOWLEDGMENTS. We thank Dr. S. Chung and Dr. C. Kothapalli for assistance in designing the microfludic device. This work was supported by Draper Laboratories University Research and Development Project N.DL-H-550151, National Cancer Institute Grant R21CA140096-01 (to J.L.C.), and the Singapore–Massachusetts Institute of Technology Alliance for Research and Technology (R.D.K). W.J.P. was supported by a National Science Foundation Graduate Research Fellowship.

1. Swartz MA, Fleury ME (2007) Interstitial flow and its effects in soft tissues. *Annu Rev Biomed Eng* 9:229–256.
2. Jain RK (1987) Transport of molecules in the tumor interstitium: A review. *Cancer Res* 47:3039–3051.
3. Boardman KC, Swartz MA (2003) Interstitial flow as a guide for lymphangiogenesis. *Circ Res* 92:801–808.
4. Jain RK (1987) Transport of molecules across tumor vasculature. *Cancer Metastasis Rev* 6:559–593.
5. Levick JR (1987) Flow through interstitium and other fibrous matrices. *Q J Exp Physiol* 72:409–437.
6. Chary SR, Jain RK (1989) Direct measurement of interstitial convection and diffusion of albumin in normal and neoplastic tissues by fluorescence photobleaching. *Proc Natl Acad Sci USA* 86:5385–5389.
7. Dafni H, Israely T, Bhujwalla ZM, Benjamin LE, Neeman M (2002) Overexpression of vascular endothelial growth factor 165 drives peritumor interstitial convection and induces lymphatic drain: Magnetic resonance imaging, confocal microscopy, and histological tracking of triple-labeled albumin. *Cancer Res* 62:6731–6739.
8. Heldin CH, Rubin K, Pietras K, Östman A (2004) High interstitial fluid pressure - an obstacle in cancer therapy. *Nat Rev Cancer* 4:806–813.
9. Curti BD, et al. (1993) Interstitial pressure of subcutaneous nodules in melanoma and lymphoma patients: Changes during treatment. *Cancer Res* 53(10, Suppl):2204–2207.
10. Chang SF, et al. (2008) Tumor cell cycle arrest induced by shear stress: Roles of integrins and Smad. *Proc Natl Acad Sci USA* 105:3927–3932.
11. Hofmann M, et al. (2006) Lowering of tumor interstitial fluid pressure reduces tumor cell proliferation in a xenograft tumor model. *Neoplasia* 8:89–95.
12. Leunig M, et al. (1992) Angiogenesis, microvascular architecture, microhemodynamics, and interstitial fluid pressure during early growth of human adenocarcinoma LS174T in SCID mice. *Cancer Res* 52:6553–6560.
13. Shields JD, et al. (2007) Autologous chemotaxis as a mechanism of tumor cell homing to lymphatics via interstitial flow and autocrine CCR7 signaling. *Cancer Cell* 11: 526–538.
14. Fleury ME, Boardman KC, Swartz MA (2006) Autologous morphogen gradients by subtle interstitial flow and matrix interactions. *Biophys J* 91:113–121.
15. Griffith LG, Swartz MA (2006) Capturing complex 3D tissue physiology *in vitro*. *Nat Rev Mol Cell Biol* 7:211–224.
16. Vickerman V, Blundo J, Chung S, Kamm RD (2008) Design, fabrication and implementation of a novel multi-parameter control microfluidic platform for three-dimensional cell culture and real-time imaging. *Lab Chip* 8:1468–1477.
17. Friedl P, et al. (1995) Migration of coordinated cell clusters in mesenchymal and epithelial cancer explants *in vitro*. *Cancer Res* 55:4557–4560.
18. Wang S, Tarbell JM (2000) Effect of fluid flow on smooth muscle cells in a 3-dimensional collagen gel model. *Arterioscler Thromb Vasc Biol* 20:2220–2225.
19. Ng CP, Swartz MA (2003) Fibroblast alignment under interstitial fluid flow using a novel 3-D tissue culture model. *Am J Physiol Heart Circ Physiol* 284:H1771–H1777.
20. Fraley SI, et al. (2010) A distinctive role for focal adhesion proteins in three-dimensional cell motility. *Nat Cell Biol* 12:598–604.
21. Li S, et al. (2002) The role of the dynamics of focal adhesion kinase in the mechanotaxis of endothelial cells. *Proc Natl Acad Sci USA* 99:3546–3551.
22. Ng CP, Hinz B, Swartz MA (2005) Interstitial fluid flow induces myofibroblast differentiation and collagen alignment in vitro. *J Cell Sci* 118:4731–4739.
23. Lin SS, et al. (2009) Topotecan inhibits cancer cell migration by down-regulation of chemokine CC motif receptor 7 and matrix metalloproteinases. *Acta Pharmacol Sin* 30:628–636.
24. Kochetkova M, Kumar S, McColl SR (2009) Chemokine receptors CXCR4 and CCR7 promote metastasis by preventing anoikis in cancer cells. *Cell Death Differ* 16: 664–673.
25. Müller A, et al. (2001) Involvement of chemokine receptors in breast cancer metastasis. *Nature* 410:50–56.
26. Brinkman HC (1947) A calculation of the viscous force exerted by a flowing fluid on a dense swarm of particles. *Appl Sci Res* A1:27–34.
27. Levesque MJ, Nerem RM (1985) The elongation and orientation of cultured endothelial cells in response to shear stress. *J Biomech Eng* 107:341–347.
28. Thomas JW, et al. (1998) SH2- and SH3-mediated interactions between focal adhesion kinase and Src. *J Biol Chem* 273:577–583.
29. Schaller MD, et al. (1994) Autophosphorylation of the focal adhesion kinase, pp125FAK, directs SH2-dependent binding of pp60src. *Mol Cell Biol* 14:1680–1688.
30. Ishida T, Peterson TE, Kovach NL, Berk BC (1996) MAP kinase activation by flow in endothelial cells. Role of beta 1 integrins and tyrosine kinases. *Circ Res* 79:310–316.
31. Li S, et al. (1997) Fluid shear stress activation of focal adhesion kinase. Linking to mitogen-activated protein kinases. *J Biol Chem* 272:30455–30462.
32. Jalali S, et al. (1998) Shear stress activates p60src-Ras-MAPK signaling pathways in vascular endothelial cells. *Arterioscler Thromb Vasc Biol* 18:227–234.
33. Brånemark PI (1965) Capillary form and function. The microcirculation of granulation tissue. *Bibl Anat* 7:9–28.
34. Li S, Huang NF, Hsu S (2005) Mechanotransduction in endothelial cell migration. *J Cell Biochem* 96:1110–1126.
35. Franke RP, et al. (1984) Induction of human vascular endothelial stress fibres by fluid shear stress. *Nature* 307:648–649.
36. Wang N, Butler JP, Ingber DE (1993) Mechanotransduction across the cell surface and through the cytoskeleton. *Science* 260:1124–1127.
37. Pedersen JA, Lichter S, Swartz MA (2010) Cells in 3D matrices under interstitial flow: Effects of extracellular matrix alignment on cell shear stress and drag forces. *J Biomech* 43:900–905.
38. Jalali S, et al. (2001) Integrin-mediated mechanotransduction requires its dynamic interaction with specific extracellular matrix (ECM) ligands. *Proc Natl Acad Sci USA* 98: 1042–1046.
39. Tzima E, del Pozo MA, Shattil SJ, Chien S, Schwartz MA (2001) Activation of integrins in endothelial cells by fluid shear stress mediates Rho-dependent cytoskeletal alignment. *EMBO J* 20:4639–4647.
40. Shyy JY, Chien S (2002) Role of integrins in endothelial mechanosensing of shear stress. *Circ Res* 91:769–775.
41. Galbraith CG, Yamada KM, Sheetz MP (2002) The relationship between force and focal complex development. *J Cell Biol* 159:695–705.
42. Kong F, García AJ, Mould AP, Humphries MJ, Zhu C (2009) Demonstration of catch bonds between an integrin and its ligand. *J Cell Biol* 185:1275–1284.
43. Fincham VJ, Frame MC (1998) The catalytic activity of Src is dispensable for translocation to focal adhesions but controls the turnover of these structures during cell motility. *EMBO J* 17:81–92.
44. Sieg DJ, et al. (1998) Pyk2 and Src-family protein-tyrosine kinases compensate for the loss of FAK in fibronectin-stimulated signaling events but Pyk2 does not fully function to enhance FAK- cell migration. *EMBO J* 17:5933–5947.
45. Lo CM, Wang HB, Dembo M, Wang YL (2000) Cell movement is guided by the rigidity of the substrate. *Biophys J* 79:144–152.
46. Lin X, Helmke BP (2009) Cell structure controls endothelial cell migration under fluid shear stress. *Cell Mol Bioeng* 2:231–243.
47. Milosevic M, et al. (2001) Interstitial fluid pressure predicts survival in patients with cervix cancer independent of clinical prognostic factors and tumor oxygen measurements. *Cancer Res* 61:6400–6405.